Reference Receiver Enhanced Digital Linearization of Wideband Direct-Conversion Receivers

Jaakko Marttila, *Member, IEEE,* Markus Allén, *Student Member, IEEE,* Marko Kosunen, *Member, IEEE* Kari Stadius, *Member, IEEE* Jussi Ryynänen, *Member, IEEE* and Mikko Valkama, *Senior Member, IEEE*

***Abstract*—This paper proposes two digital receiver (RX) linearization and I/Q correction solutions, where an additional reference RX (ref-RX) chain is adopted in order to obtain a more linear observation, in particular, of the strong incoming signals. This is accomplished with reduced RF gain in the ref-RX in order to avoid nonlinear distortion therein. In digital domain, the signal observed by the ref-RX is exploited in linearizing the main RX. This allows combining the sensitivity of the main RX and the linearity of the lower-gain ref-RX. The proposed digital processing solutions for implementing the linearization are feed-forward interference cancellation and nonlinearity inversion, which are both adapted blindly, without *a priori* information of the received signals or RX nonlinearity characteristics. The linearization solutions enable flexible suppression of nonlinear distortion stemming from both the RF and analog baseband components of different orders. Especially wideband multi-carrier RXs, where significant demands are set for the RX linearity and I/Q matching, are targeted. Using comprehensive RF measurements and realistic base-station scale components, an RX blocker tolerance improvement of $23\,\mathrm{dB}$ and weak carrier signal-to-noise-and-distortion ratio gain of $19\,\mathrm{dB}$ are demonstrated with combined linearization and I/Q correction.**

***Index Terms*—adaptive signal processing, direct-conversion receiver, interference cancellation, intermodulation distortion, I/Q imbalance, linearization techniques, mirror-frequency interference, nonlinear distortion, radio receiver.**

I. Introduction

WIDEBAND multi-carrier or multi-channel direct-conversion receivers (DCRs) are becoming increasingly popular while the cost and size of a single receiver (RX) chain are dropping due to advances in circuit design and underlying process technologies. Also multi-operator and/or multi-technology scenarios, where signals of multiple operators and potentially of multiple radio access networks are all received simultaneously with a single wideband RX hardware are becoming more common. In such conditions, the power range of the strong and weak carriers inside, e.g., $100\,\mathrm{MHz}$ reception band, can be up to 60–$70\,\mathrm{dBs}$ [1]–[3]. This is especially emphasized in future ultra-dense networks [4], where the strong, blocking mobile transmitters can be in very close proximity of the base-station (BS) RX [3] while the weak carriers are received through multiple shadowing obstacles. This sets stringent requirements for the RX linearity. Improving the linearity by analog means is challenging, especially with strict limitations for the design and implementation costs, circuit size and power consumption. [5]–[7]. However, the requirements for analog hardware can be effectively alleviated by means of digital signal processing (DSP) [8]–[13]. This allows the received signal quality to be enhanced after the analog RX with digital post-processing solutions.

A widely-adopted DCR [5], [14] is illustrated at conceptual level in Fig. 1, where the most important nonlinear distortion and mirror-frequency interference (MFI) sources are highlighted. To reflect the overall distortion characteristics as accurately as possible, the nonlinear distortion modeling in this paper covers arbitrary-order nonlinearities both in the RF as well as the baseband (BB) components. In addition to the actual nonlinear distortion products, MFI components are induced by the in-phase/quadrature (I/Q) mismatches of the down-converting mixers and other analog components in the BB I and Q rails [8]. Hence, to account for all these distortion products, we derive the overall nonlinear behavioral model for the RX, employing elementary nonlinear transformations of the complex-valued signal and its complex-conjugate.

Two alternative DSP solutions are then derived using the behavioral model in order to either (*i*) cancel or (*ii*) invert all the essential nonlinear distortion effects due to the analog hardware. The first method is called reference-receiver-enhanced adaptive interference cancellation (RR-AIC), where an estimate of the nonlinear distortion is generated based on the more linear reference receiver (ref-RX) observation and then subtracted from the main RX signal. In the second method, called reference-receiver-aided nonlinearity inversion (RR-INV), an explicit inverse for the overall nonlinearity of the DCR is pursued, using the ref-RX observation as a calibration signal.

The rest of this paper is organized as follows. Section II presents the prior-art and highlights the novelty of the proposed solutions. In Section III, arbitrary-order modeling of nonlinear distortion and MFI appearing in wideband DCRs is carried out. Building on this modeling, Sections IV and V propose then two linearization solutions based on the distortion cancellation and nonlinearity inversion ideas, respectively. Therein, also digital parameter estimation and learning solutions are addressed. True RF measurements are presented and analyzed in Section VI, comparing the performance of the proposed solutions to the state-of-the-art. Section VII further discusses the benefits and costs of the proposed solutions. Finally, conclusions are drawn in Section VIII.

This work was supported by Nokia Networks and the Finnish Funding Agency for Technology and Innovation (Tekes).

J. Marttila, M. Allén and M. Valkama are with the Department of Electronics and Communications Engineering, Tampere University of Technology, Korkeakoulunkatu 1, 33720 Tampere, Finland. E-mail: jaakko.marttila@tut.fi, markus.allen@tut.fi and mikko.e.valkama@tut.fi.

M. Kosunen, K. Stadius and J. Ryynänen are with Department of Micro- and Nanosciences, Aalto University School of Electrical Engineering, Otakaari 5, 02150 Espoo, Finland. E-mail: kari.stadius@aalto.fi, marko.kosunen@aalto.fi, jussi.ryynanen@aalto.fi

II. Prior-Art in Digital Receiver Linearization

RX linearization through post-processing has been addressed to some extent already in the existing literature. In [12], [15], the nonlinear distortion estimate is generated on the analog RF and then digitized with separate RX chains. This needs specific RX hardware with analog cubing and squaring operators, does not consider the modeling or suppression of the BB nonlinearities and only approximately estimates higher than third-order distortion. In addition, analog implementation of the cubing and squaring operators contains inherent inaccuracies. Also [13] considers adopting an additional RX chain but aims only at suppressing the intermodulation distortion (IMD) appearing at the RF, and thus neglects the effects of BB nonlinearities and I/Q mismatch. Furthermore, only computer simulations based results are reported.

In addition, some single-RX based adaptive interference cancellation (AIC) methods for RX linearization have been proposed, e.g., in [16]–[22]. In these works, the reference for the nonlinear distortion estimation and cancellation is generated from the main received signal through simple linear filtering. This inherently gives only approximate distortion estimates, because the inband portion of the nonlinear distortion degrades the quality of the reference signal. In addition, knowledge of the blocker center frequencies and bandwidths need to be obtained and the filters for picking these blockers need to be either designed and optimized in real-time or stored in a filter bank to be able to consider different signal scenarios. In [23], on the other hand, a single-RX based digital post-inverse solution for nonlinear distortion suppression is described. The proposed solution, however, is not able to consider frequency-selective nature of the distortion induced by the analog hardware. In addition, the precision of the discrete-cosine-transform applied is limiting the suppression performance and robustness of the adaptation.

A reference analog-to-digital converter (ADC) based solution for suppressing the ADC nonlinearities only is proposed in [24]. However, the nonlinearities of the preceding RX front-end are not considered in any manner.

A post-inverse linearization solution with offline calibration, where the transmitter of the transceiver unit is used to feed in the calibration signal in order to find the parameters of the post-inverse nonlinearity is proposed in [25]. This, however, requires specific calibration periods and thus limits the adaptability and flexibility of the solution.

The solutions proposed in this paper are able to overcome the limitations of the prior art elaborated above. The proposed solutions are blind and can be adapted online, during the normal RX operation. The nonlinear distortion regeneration and suppression are done fully on the digital BB. From the analog hardware point-of-view, another parallel RX chain is used as a ref-RX. This ref-RX is assumed to have the same reception bandwidth as the main RX. Otherwise, no specific RX design or tailoring is needed. For example, commercial off-the-shelf dual-RX set-ups can be utilized for this purpose. In general, the proposed solutions enable combining the sensitivity of the main RX and the linearity of the lower-gain ref-RX in a flexible manner. Furthermore, opposed to [16]–[22], the receiver linearization solutions proposed in this paper can also facilitate digital out-of-band blocker cancellation, by tuning the ref-RX center-frequency accordingly.

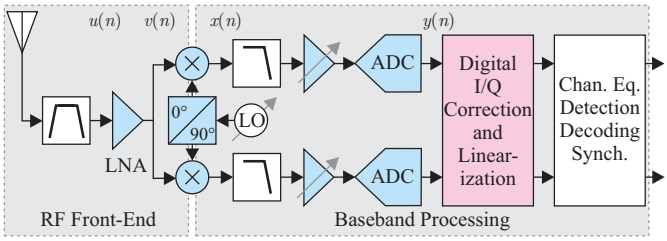

Fig. 1. Conceptual DCR block diagram emphasizing the main sources of nonlinear distortion and I/Q mismatch together with the employed baseband-equivalent discrete-time mathematical notation.

In general, it is known that the down-scaling of the semiconductor processes and decreasing supply voltages exacerbates the noise and linearity performance of analog signal processing electronics, while largely benefiting DSP implementations from speed and power consumption point-of-view. This trend will make the digital error correction and linearization more and more viable solution in the future, but is already used, for example, in linearization of ADCs [26]. Furthermore, digital predistortion (DPD), relying on similar behavioral modeling principles and an additional observation RX, is already widely applied in linearizing transmitter power amplifiers [27]. Finally, it is noted that there are also some works in the literature [28]–[31] that consider specifically the modeling and suppression of the self-interference induced by the own transmitter, in particular in frequency division duplexing devices. While in such scenarios the reference signal for cancellation is inherently available, the work in this paper considers more generic problem setting with arbitrary and unknown strong waveforms entering the RX. These approaches could be potentially combined, for achieving versatile and efficient distortion suppression at the RX.

III. Arbitrary-Order Nonlinearity Modeling for Direct-Conversion Receiver

In this section, mathematical modeling of a wideband DCR, illustrated in Fig. 1, is presented. Both the nonlinearities and I/Q mismatches of the analog processing stages are considered. The baseband-equivalent signal model for a DCR is visualized in Fig. 2, together with illustrative spectral examples showing a scenario where, for simplicity of visualization, only a single received carrier is depicted, being located at a small intermediate frequency (IF) after the RF down-conversion stage. In general, arbitrary-order nonlinearities are considered for both the RF and BB, in order to provide a complete and comprehensive behavioral model of the overall RX.

A. LNA Modeling

The RF low-noise amplifier (LNA) nonlinearities are modeled with an odd-order memory polynomial incorporating separate memory filters for the different polynomial components in order to cover different nonlinearity orders and the

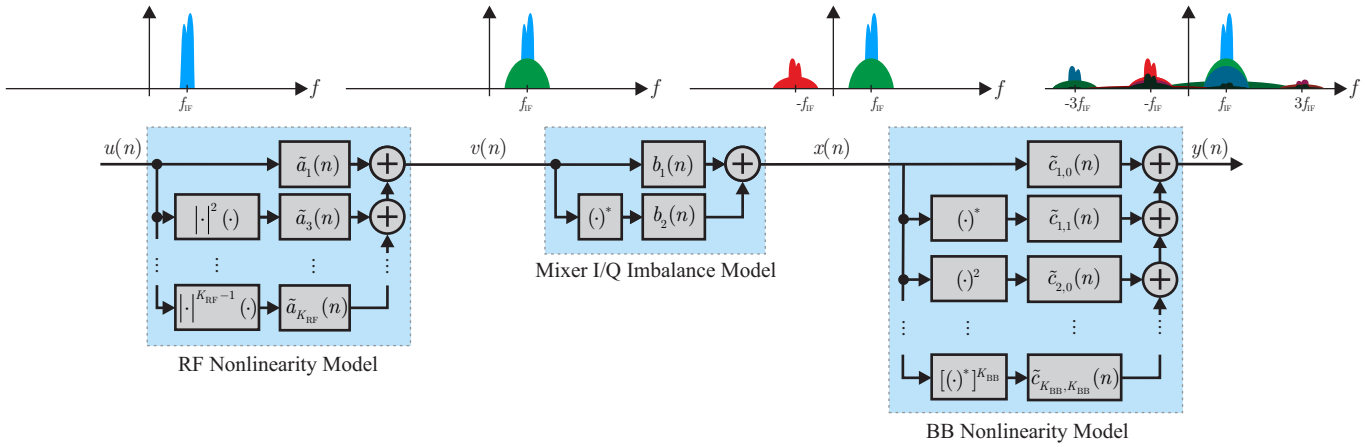

Fig. 2. Illustration of cascaded parallel Hammerstein models considering RF and BB nonlinearities as well as mixer and BB I/Q mismatches. The highest nonlinearity orders taken into account for the RF and the BB are K_{RF} and K_{BB}, respectively. Due to the generality of the nonlinearity models, they also take mixer nonlinearities into account. The spectrum illustrations are sketched for BB equivalent signals matching to the mathematical modeling in the paper, and only a single carrier located at the f_{IF}, after I/Q down-conversion, is shown for visualization purposes.

related memory effects as accurately as possible. This structure is known as parallel Hammerstein model [32], [33] and is illustrated in Fig. 2. The choice of odd-order simplification is justified by even order distortion falling either on multiples of the RF center frequency or around BB, while the interesting signals at this stage are still at RF. In addition, also the odd-order harmonic components are excluded based on the same assumptions [34]. This is a valid approach as long as the center frequency is high compared to the instantaneous bandwidth of the total signal entering the LNA. However, if the reception band becomes very wide, e.g., in gigahertz range, in respect to the center frequency, also harmonic distortion should be considered.

Mathematically, the odd polynomial orders, considered up to K_{RF}, are gathered into Ω_{RF}, i.e., $\Omega_{\text{RF}} = \{1, 3, ..., K_{\text{RF}}\}$. With this assumption, the LNA output as a discrete-time baseband-equivalent model can be expressed as

$$\begin{aligned} v(n) &= \sum_{k\in\Omega_{\text{RF}}} a_k(n) * \frac{1}{2^{k-1}} \binom{k}{\frac{k+1}{2}} [u(n)u^*(n)]^{(k-1)/2} u(n) \\ &= \sum_{k\in\Omega_{\text{RF}}} \tilde{a}_k(n) * |u(n)|^{k-1} u(n), \end{aligned} \tag{1}$$

where $a_k(n)$ are the impulse-responses for each odd polynomial order in Ω_{RF} taking memory effects into account and $u(n)$ is the original LNA input. Notationwise, $*$ and $(\cdot)^*$ denote convolution and complex-conjugate, respectively. Furthermore, the modified filters, denoted by $\tilde{a}_k(n)$, include also the contribution of the scalar scaling coefficients multiplying the signal component on the first line of (1). Using these impulse-responses instead of scalar coefficients extends the modeling presented in [34] to cover also memory effects. In addition, using complex-valued impulse-response taps allows covering AM/PM characteristics of the amplifiers [35]. For Ω_{RF}, one practical example is third order distortion modeling, $\Omega_{\text{RF}} = \{1, 3\}$, where 1 represents the linear component. Such simplified modeling was earlier assumed, e.g., in [18], [20], [25].

B. I/Q Mixer and Baseband Component Modeling

Next, the LNA output is fed into down-converting I/Q mixers. The finite image-rejection ratio (IRR) of the mixers is modeled by adding a filtered complex-conjugate of the input signal to the output of the mixer [8], [36]. In this way, the mixer output signal becomes

$$x(n) = b_1 v(n) + b_2 v^*(n), \tag{2}$$

where b_1 and b_2 are the scaling coefficients for the direct and conjugate branches, being more specifically defined as $b_1 = (1 + ge^{-j\phi})/2$ and $b_2 = (1 - ge^{j\phi})/2$, where g and ϕ are the gain mismatch and the phase mismatch between the branches, respectively [8], [36]. The nonlinearity of the I/Q mixers and the I/Q mismatches between the BB I and Q component frequency responses are included in the following BB nonlinearity model and are thus not explicitly included in the instantaneous mixer I/Q mismatch model in (2).

Finally, the BB I and Q nonlinearities are included in the joint model. Independent arbitrary order parallel Hammerstein models are employed for modeling both the rails in order to take into account also the possible I/Q mismatches between the rails. The nonlinearities can originate from I/Q mixers, BB amplifiers and ADCs. In the BB stage modeling, also even order nonlinearities are taken into account, modeling, e.g., the self-mixing problem in the mixer [8]. Similar to the RF, the orders included in the modeling, up to K_{BB}, are represented with Ω_{BB}. In practice, this can be, e.g., $\Omega_{\text{BB}} = \{1, 2, 3\}$ for modeling second- and third-order BB nonlinear distortion. The

final digitized waveform can thus be expressed as

$$\begin{aligned} y(n) &= \sum_{k\in\Omega_{\text{BB}}} c_{\text{re},k}(n) * x_{\text{I}}^{k}(n) + jc_{\text{im},k}(n) * x_{\text{Q}}^{k}(n) \\ &= \sum_{k\in\Omega_{\text{BB}}} \frac{1}{2^k} \sum_{l=0}^{k} \left[\left(c_{\text{re},k}(n) + \frac{(-1)^l c_{\text{im},k}(n)}{j^{k-1}} \right) \right. \\ &\qquad \left. * \binom{k}{l} x^{k-l}(n)[x^*(n)]^l \right] \\ &= \sum_{k\in\Omega_{\text{BB}}} \sum_{l=0}^{k} \tilde{c}_{k,l}(n) * x^{k-l}(n)[x^*(n)]^l, \end{aligned} \tag{3}$$

where $c_{\text{re},k}(n)$ and $c_{\text{im},k}(n)$ are the impulse responses for each polynomial order defined in Ω_{BB} for I and Q rails, respectively, taking memory effects into account. In addition, $\tilde{c}_{k,l}(n)$ are the modified filters including also the scalar multipliers on second line of (3), reflecting the combined responses for each of the complex-valued signal components.

C. Cascaded Effects of RF and BB Nonlinearities

The signal components resulting from the *cascaded effects* of (1)–(3) are gathered into Table I, in terms of the ideal RX input signal $u(n)$, in the example case of $\Omega_{\text{RF}} = \{1, 3\}$ and $\Omega_{\text{BB}} = \{1, 2, 3\}$, together with short description of each component. Even though differential signaling is known to reduce even-order distortion components, the second-order term is included in the BB part since, e.g., mixer-induced second-order distortion can still be relevant in certain scenarios [37]. These components and the presented modeling form the basis for developing the linearization approaches described in the following sections. In Table I, the first-column components ("Terms") appear purely due to the nonlinearities. The second-column components ("Mirror Terms") appear only in case of I/Q mismatch either in the mixers or the BB I and Q rails. In (2)–(3), this means that the respective scaling coefficients and impulse responses go to zero in case of perfect I/Q matching. In addition, if all the orders considered in the BB nonlinearity modeling include I/Q mismatch, introducing mixer I/Q mismatch does not generate new Mirror Terms but only affects the effective responses of the ones already appearing because of BB I/Q mismatches. It should be noted that the Terms in Table I cannot be strictly separated into RF distortion and BB distortion, even when the modeling of those stages differs in ways described in (1)–(3). For example, the Term $|u(n)|^2u(n)$ is stemming from both the third-order RF nonlinearity, described by (1) and the third-order BB nonlinearity, described by (3). The proportions of these contributions depend on the characteristics of the exact hardware at hand and, thus, the exact coefficients of (1)–(3).

Generally, the list of distortion components with differing orders considered in the modeling can be obtained by evaluating (1)–(3) in symbolic form. This can be carried out either with pen and paper or using software tools, such as MATLAB Symbolic Math Toolbox.

Notice that the above modeling results are generic and apply to arbitrary LNA input signal $u(n)$, independently of whether receiving a single carrier or multiple carriers, or whether the (composite) received signal after I/Q down-conversion is located strictly at baseband or not. The graphical illustration in Fig. 2 emphasizes the creation of different distortion terms due to an individual strong incoming carrier which is located at f_{IF} after the I/Q down-conversion stage.

TABLE I
TERMS GENERATED BY THE JOINT NONLINEARITY MODEL IN CASE OF $\Omega_{\text{RF}} = \{1, 3\}$ AND $\Omega_{\text{BB}} = \{1, 2, 3\}$

Terms	Mirror Terms	Interpretation
$u(n)$	$u^*(n)$	Original signal around f_{IF}
$\lvert u(n)\rvert^2$	-	2nd-order IMD around BB
$u^2(n)$, $[u^*(n)]^2$	-	2nd-order harmonics around $\pm 2f_{\text{IF}}$
$\lvert u(n)\rvert^2u(n)$	$\lvert u(n)\rvert^2u^*(n)$	3rd-order IMD around f_{IF}
$[u^*(n)]^3$	$u^3(n)$	3rd-order harmonics around $-3f_{\text{IF}}$
$\lvert u(n)\rvert^4$	-	4th-order IMD around BB
$\lvert u(n)\rvert^2u^2$, $\lvert u(n)\rvert^2[u^*(n)]^2$	-	3rd-order IMD around $\pm f_{\text{IF}}$
$\lvert u(n)\rvert^4u(n)$	$\lvert u(n)\rvert^4u^*(n)$	5th-order IMD around f_{IF}
$\lvert u(n)\rvert^2[u^*(n)]^3$	$\lvert u(n)\rvert^2u^3(n)$	3rd-order IMD around $-3f_{\text{IF}}$
$\lvert u(n)\rvert^6$	-	6th-order IMD around BB
$\lvert u(n)\rvert^4u^2$, $\lvert u(n)\rvert^4[u^*(n)]^2$	-	5th-order IMD around $\pm 2f_{\text{IF}}$
$\lvert u(n)\rvert^6u(n)$	$\lvert u(n)\rvert^6u^*(n)$	7th-order IMD around f_{IF}
$\lvert u(n)\rvert^4[u^*(n)]^3$	$\lvert u(n)\rvert^4u^3(n)$	5th-order IMD around $-3f_{\text{IF}}$
$\lvert u(n)\rvert^8u(n)$	$\lvert u(n)\rvert^8u^*(n)$	9th-order IMD around f_{IF}
$\lvert u(n)\rvert^6[u^*(n)]^3$	$\lvert u(n)\rvert^6u^3(n)$	7th-order IMD around $-3f_{\text{IF}}$

IV. PROPOSED REFERENCE RECEIVER ENHANCED ADAPTIVE INTERFERENCE CANCELLATION (RR-AIC) SOLUTION FOR WIDEBAND LINEARIZATION

In this section, the proposed RR-AIC linearization solution is described in detail, building on the modeling results of the previous section. In the RR-AIC another parallel RX, in which the RF LNA stage is excluded, is employed as illustrated in Fig. 3. Thus, this ref-RX is not creating RF nonlinear distortion and is operating in more linear region when it comes to the I/Q mixer and BB stages. With the ref-RX, only the strongest blockers need to be observed, to be used as a reference signal in the digital linearization processing. Thus, the ref-RX noise figure and the quantization resolution of the corresponding ref-RX ADC are not as critical as for the main RX, who needs to be able to receive also the weak carriers present within the reception band. The weak carriers, however, have only very little contribution to the nonlinear distortion appearing in the main RX.

The I/Q correction stage illustrated in Fig. 3 is implemented in both the main RX and the ref-RX based on [36] and applies adaptive circularity restoring MFI suppression principle. Also in the ref-RX, even though it is operated on a more linear region than the main RX, the MFI contribution might be significant. In order to achieve as high quality reference signal as possible, it is thus desirable to perform I/Q correction

therein as well. The MFI suppression is generally focusing on the contribution of the possible I/Q mismatch induced Mirror Terms in Table I. This approach is validated by the fact that all the Mirror Terms in Table I can be modeled as BB induced MFI. Thus, the MFI appearing at the last stage of the analog front-end is suppressed first in the digital front-end, while the actual nonlinearities are tackled thereafter. The MFI suppression performance will be demonstrated using the RF measurements in Sections VI, together with the linearization performance. The aim of the actual linearization stage, which is one of the main contributions in this paper, is to suppress the remaining nonlinear Terms in Table I.

In Fig. 3, the RR-AIC stages, namely the reference nonlinearities, adaptive filtering and interference cancellation are illustrated. These stages aim at regenerating and cancelling the nonlinear distortion induced by the analog RX components. This is based on the mathematical modeling presented in Section III and discussed in more detail in the following. The description in this section follows the signal flow and notations illustrated in Fig. 3.

A. Reference Nonlinearities

In the reference nonlinearity stage, shown in Fig. 3, elementary nonlinear transformations of the I/Q corrected ref-RX signal $\hat{u}(n)$ are generated. Herein, the nonlinearity model is assumed to be a parallel Hammerstein model [32], [33] but, generally, any nonlinearity model can be applied. However, a polynomial model followed by a filtering stage has the benefit of being linear in parameters and is thus very well suitable for adaptive parameter learning. The exact choice of the model in individual scenarios should be done based on the hardware at hand and the desired performance/complexity trade-off. For example, a simplified polynomial model followed by scalar adaptive coefficients could be employed, if considering memory effects of the analog front-end components is not seen necessary.

In Fig. 3, the reference nonlinearities are denoted with $f_0(\cdot), f_1(\cdot), ..., f_P(\cdot)$, where P is the number of nonlinear terms and $f_0(\cdot)$ is a linear function. Thus, the linear component signal $d_0(n)$ and the nonlinear components $d_1(n)$ to $d_P(n)$ are obtained. Here, the reference nonlinearities are chosen based on the wideband DCR modeling in the previous section. In practice, the nonlinear Terms gathered in the first column of Table I are targeted and the component signals are thus expressed as

$$\begin{aligned} d_0(n) &= f_0(\hat{u}(n)) = \hat{u}(n), \\ d_1(n) &= f_1(\hat{u}(n)) = \hat{u}^2(n), \\ d_2(n) &= f_2(\hat{u}(n)) = [\hat{u}^*(n)]^2, \\ &\vdots \\ d_P(n) &= f_P(\hat{u}(n)) = \dots \end{aligned} \tag{4}$$

In general, the nonlinearity modeling in here should match the actual main DCR characteristics as accurately as possible. Similar to the choice of the nonlinearity modeling approach in general, also the employed reference nonlinearities should be optimized based on the performance/complexity trade-off. The optimum set of reference nonlinearities depends also on the given RX hardware at hand. Thus, giving universal set of reference nonlinearities is not seen feasible. At the same time, reducing the number of kernels in the following learning stage can be approached using, for example, principal component analysis in similar manner as has been proposed for digital predistortion of power amplifier nonlinearities [41]. Furthermore, the role of different nonlinearity components has been studied in [20] in a simplified two-tone reception scenario, giving insight to the significance of each component. The role of this selection is also illustrated in Section VI together with the linearization results.

The produced nonlinear components are next fed in parallel to the adaptive filtering stages, as illustrated in Fig. 3. This allows individual adaptive weighting for each of the distortion components. The combined, adaptively filtered nonlinear components yield then the actual estimate of the overall prevailing nonlinear distortion in the received main RX signal. Notice that the linear component is naturally excluded from the actual cancellation signal but is deliberately included in the generation of the error signal for adapting the filters, in order to avoid bias in the adaptive filter coefficients [38] because of the correlation between the nonlinear components and the linear component present in the original main RX signal. Other alternative option could be to adopt an additional orthogonalization stage after the generation of the basic reference nonlinearities or nonlinear basis functions.

In general, in order to mimic the nonlinearities in the analog front-end, no harmful aliasing should be allowed in the digital reference nonlinearities. In this scenario, the harmful aliasing means distortion components that alias inside the actual reception and cancellation bandwidth. This can be avoided by first interpolating $\hat{u}(n)$, feeding it to the nonlinear operators $f_1(\cdot), f_2(\cdot), ..., f_P(\cdot)$ and then filtering and decimating the generated nonlinear components back to the original sample rate. In this way, if non-harmful aliasing is allowed, the necessary high sample rate is $f_{\text{S,high}} = [(K+1)/2]B$, where K and B are the highest polynomial order applied and the reception bandwidth dictated by the ADC and the analog filtering, respectively [10]. If no aliasing is allowed at all, the necessary sample rate is $f_{\text{S,high}} = KB$. The need for increased sample rate is illustrated in Fig. 3 with a dashed-line box.

B. Parameter Learning and Interference Cancellation

The general principle for learning the adaptive filter coefficients is to minimize the error power between the sum of the adaptively filtered parallel reference nonlinearity output signals and the received main RX signal. The intuition behind the idea is to find a black-box parallel Hammerstein model for the main RX analog parts and use the nonlinear components of the model to cancel the nonlinear distortion from the received signal. This is accomplished by subtracting the adaptively filtered nonlinear components from the received main RX signal. In general, the adaptive filters are used to find optimal amplitude and phase responses for the nonlinear components,

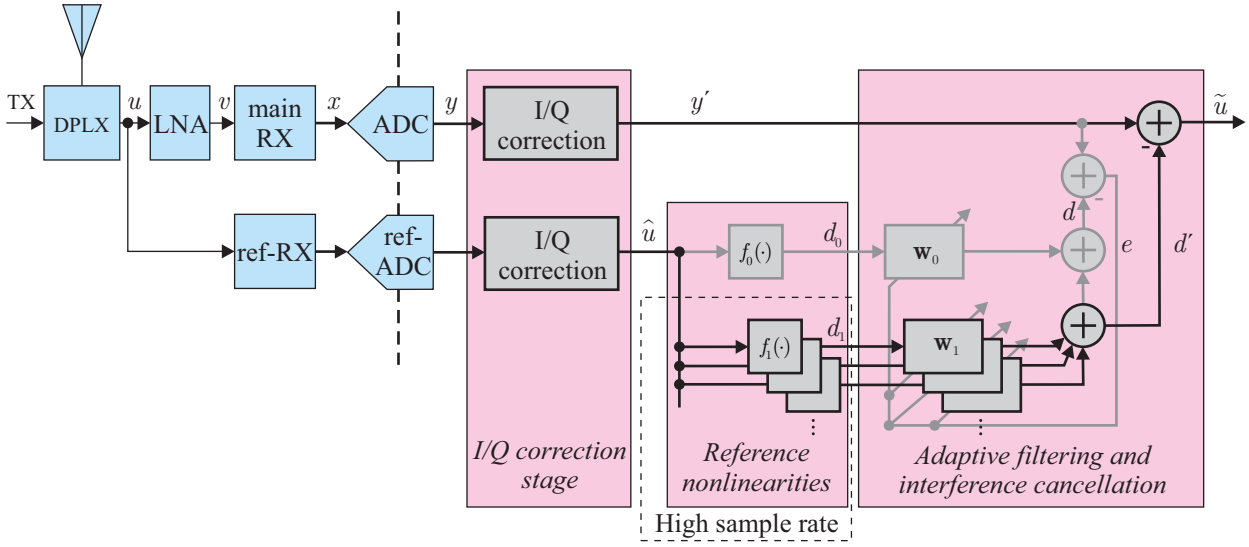

Fig. 3. Block diagram illustrating the principle of the proposed RR-AIC method for main RX I/Q correction and linearization. The MFI suppression and nonlinearity cancellation stages are cascaded. The I/Q correction stage is implemented based on [36]. The time index n is omitted from the signal notation for illustration convenience.

thus creating an optimal estimate of the nonlinear distortion induced in the main RX analog front-end. In practice, the learning can build on, e.g., least-squares (LS) block solution, recursive least squares (RLS) or sample-wise least-mean square (LMS) adaptation [38]. In the following, the LS block solution is described in detail, as an illustrative example. Generally, also other learning algorithms can be applied.

First, the set of filters $\mathbf{w}_0, \mathbf{w}_1, ..., \mathbf{w}_P$, depicted also in Fig. 3, is optimized in the LS sense with the given block of data. This block can be, e.g., a frame of the received signal, and its length is denoted by N. The length of each filter is M and hence, e.g., $\mathbf{w}_1 = [w_1(1), w_1(2), ..., w_1(M)]^{\mathrm{T}}$. The filters are obtained by solving the model fitting problem

$$\arg\min_{\mathbf{w}_{\mathrm{C}}} \|\mathbf{D}_{\mathrm{C}}\mathbf{w}_{\mathrm{C}} - \mathbf{y}'\|^2 \tag{5}$$

for $\mathbf{w}_{\mathrm{C}}= [\mathbf{w}_0^{\mathrm{T}}, \mathbf{w}_1^{\mathrm{T}} ..., \mathbf{w}_P^{\mathrm{T}}]^{\mathrm{T}}$ such that it minimizes the power of $\mathbf{D}_{\mathrm{C}}\mathbf{w}_{\mathrm{C}} - \mathbf{y}'$, which is the modeling error. This can be interpreted as fitting the linear component and the nonlinear components with memory size M and individual weights to the I/Q corrected main RX signal block $\mathbf{y}' = [y'(1), y'(2), ..., y'(N)]^{\mathrm{T}}$ in LS sense. The matrix $\mathbf{D}_{\mathrm{C}}$ consists of the linear component and all the nonlinear transformations obtained via the ref-RX with M separate delays as columns as shown in (8). The resulting $\mathbf{w}_{\mathrm{C}}^{\mathrm{LS}}$ contains coefficients for all the $P+1$ filters $\mathbf{w}_0^{\mathrm{LS}}, \mathbf{w}_1^{\mathrm{LS}}, ..., \mathbf{w}_P^{\mathrm{LS}}$, having dimensions $M(P+1) \times 1$. In practice, $\mathbf{w}_{\mathrm{C}}^{\mathrm{LS}}$ is obtained by calculating the pseudo-inverse of $\mathbf{D}_{\mathrm{C}}$ [38], giving

$$\begin{aligned} \mathbf{w}_{\mathrm{C}}^{\mathrm{LS}} &= \mathbf{D}_{\mathrm{C}}^{+}\mathbf{y}' \\ &= (\mathbf{D}_{\mathrm{C}}^{\mathrm{H}}\mathbf{D}_{\mathrm{C}})^{-1}\mathbf{D}_{\mathrm{C}}^{\mathrm{H}}\mathbf{y}'. \end{aligned} \tag{6}$$

In general, the interference cancellation is then accomplished by subtracting the distortion estimate provided by the filters $\mathbf{w}'_{\mathrm{C}} = [\mathbf{w}_1^{\mathrm{T}}, \mathbf{w}_2^{\mathrm{T}} ..., \mathbf{w}_P^{\mathrm{T}}]^{\mathrm{T}}$ from the main RX signal $\mathbf{y}'$, written here as

$$\tilde{\mathbf{u}} = \mathbf{y}' - \mathbf{D}'_{\mathrm{C}}\mathbf{w}'_{\mathrm{C}}, \tag{7}$$

which yields the linearized signal $\tilde{\mathbf{u}}$. Here, opposed to the previous model fitting stage, the actual cancellation builds on processing the nonlinear terms only, i.e., $\mathbf{D}'_{\mathrm{C}}$ is obtained from $\mathbf{D}_{\mathrm{C}}$ in (8) by removing the linear signal terms. Furthermore, in the actual online linearization after having estimated the filters $\mathbf{w}_1, \mathbf{w}_2, ..., \mathbf{w}_P$ as described above, linearization can be carried out sample by sample without any block-structure.

$$\mathbf{D}_{\mathrm{C}} = \begin{bmatrix} d_0(1) & d_0(N) & \dots & d_0(N-M+1) & d_1(1) & \dots & d_1(N-M+1) & \dots & d_P(1) & \dots & d_P(N-M+1) \\ d_0(2) & d_0(1) & & d_0(N-M+2) & d_1(2) & & d_1(N-M+2) & & d_P(2) & & d_P(N-M+2) \\ \vdots & d_0(2) & & \vdots & \vdots & & \vdots & & \vdots & & \vdots \\ & \vdots & & d_0(N) & & & d_1(N) & & & & d_P(N) \\ & & & d_0(1) & & & d_1(1) & & & & d_P(1) \\ & & & d_0(2) & & & d_1(2) & & & & d_P(2) \\ & & & \vdots & & & \vdots & & & & \vdots \\ d_0(N) & d_0(N-1) & \dots & d_0(N-M) & d_1(N) & \dots & d_1(N-M) & \dots & d_P(N) & \dots & d_P(N-M) \end{bmatrix} \tag{8}$$

V. Proposed Reference Receiver Enhanced Nonlinearity Inversion (RR-INV) Solution for Wideband Linearization

In case of nonlinearity inversion based main RX linearization approach, described in this section, the more linear perception of the received signal provided by the ref-RX is used as a calibration signal. This means that the output of the inverse nonlinearity, being fed with the main RX signal observation, is eventually mimicking this more linear observation. In this way, the ref-RX enhances also the performance of the nonlinearity inversion.

In Fig. 4, this approach is illustrated. Therein, the I/Q correction stage is first used to suppress mirror-frequency components induced by the I/Q mismatches of both the main RX and the ref-RX chain analog components. Again, the I/Q correction stage is implemented based on [36] and is assumed to tackle the Mirror Terms of Table I, as discussed in the case of RR-AIC in Section IV. The following inverse nonlinearity stage aims then in suppressing the nonlinear distortion present in the main RX observation, thus suppressing the remaining nonlinear Terms in Table I.

In the following, the RR-INV processing stages shown in Fig. 4 are described in more detail. The description follows the signal flow and notations of Fig. 4.

A. Inverse Nonlinearity

The actual nonlinearity is implemented as a memory polynomial with $P+1$ separate reference nonlinear transformation stages or basis functions $f_0(y'(n))$ to $f_P(y'(n))$, as illustrated in Fig. 4, followed by linear filters $\mathbf{w}_0, \mathbf{w}_1, ..., \mathbf{w}_P$. The value of P is not restricted to be the same as in the interference cancellation solution discussed in the previous section. The target is generally to find the reference nonlinearities which invert the effect of nonlinearity occurring in the main RX front-end.

The exact choice of the basis functions in the inverse nonlinearity solution depends on the characteristics of the forward nonlinearity whose distortion effects are to be inverted. For example, in case of a nonlinear system described by a simple power series of increasing polynomial orders, also the inverse nonlinearity can take a form of a power series [39]. The order of this inverse nonlinearity can, however, differ from the order of the original system. Thus, considering the nonlinearities in a wideband DCR, the applied basis functions are chosen from Table I also in the case of nonlinearity inversion. With these reference nonlinearities, the $P+1$ component signals $d_0(n)$ to $d_P(n)$ are obtained. Summing the component signals together, after being properly filtered, forms the final linearized signal, as shown in Fig. 4.

Proper oversampling should again be applied before the reference nonlinearities in order to avoid harmful aliasing in the component signals $d_0(n), d_1(n)..., d_P(n)$. This is highlighted in Fig. 4 with a dashed line box indicating the need for higher sampling rate. The same interpolation factor demand of $(K+1)/2$, where K is the highest considered polynomial order, discussed in Section IV, applies also herein.

B. Parameter Learning

The general principle for adapting the filters of the inverse nonlinearity is to minimize the difference of the output and the more linear signal observation captured with the ref-RX. The higher linearity of the ref-RX observation is assumed because of the reduced RF gain in the ref-RX branch. The concept is implemented in practice by subtracting this more linear blocker observation, denoted as $\hat{u}(n)$, from the inverse nonlinearity output $\tilde{u}(n)$, resulting in an error signal $e(n)$ containing only an estimate of the prevailing nonlinear distortion in $\tilde{u}(n)$. Thus, by adapting the inverse nonlinearity filters $\mathbf{w}_0, \mathbf{w}_1, ..., \mathbf{w}_P$ such that the power of this error signal is minimized, the inverse nonlinearity output is driven towards the more linear ref-RX observation while at the same time maintaining the better signal-to-noise ratio (SNR) and sensitivity of the main RX observation.

Next, we formulate the actual adaptation or parameter learning processing in more detail, again adopting the block LS principle as a concrete example. Generally, also other, e.g., sample-adaptive, learning algorithms can be applied.

The filters $\mathbf{w}_0, \mathbf{w}_1..., \mathbf{w}_P$, shown in Fig. 4, are found through LS model fitting over the given processing block. They are obtained by solving the model fitting problem

$$\arg\min_{\mathbf{w}_\mathrm{I}} \|\mathbf{D}_\mathrm{I}\mathbf{w}_\mathrm{I} - \hat{\mathbf{u}}\|^2 \tag{9}$$

for $\mathbf{w}_\mathrm{I} = [\mathbf{w}_0, \mathbf{w}_1, ..., \mathbf{w}_P]^\mathrm{T}$ in such a way that the power of the difference $\mathbf{D}_\mathrm{I}\mathbf{w}_\mathrm{I} - \hat{\mathbf{u}}$, which is the adaptation error, is minimized. Formally, the structure of the data matrix $\mathbf{D}_\mathrm{I}$ is identical to that of $\mathbf{D}_\mathrm{C}$ in (8). It should be, however, noted that here the component signals from $d_0(n)$ to $d_P(n)$, and thus also the matrix $\mathbf{D}_\mathrm{I}$, are formed by feeding the received main RX observation $y'(n)$ to the reference nonlinearities, as shown in Fig. 4. In practice, the LS optimum filters $\mathbf{w}_\mathrm{I}^\mathrm{LS}$ can be found by calculating the pseudo-inverse of $\mathbf{D}_\mathrm{I}$, expressed here as

$$\begin{aligned} \mathbf{w}_\mathrm{I}^\mathrm{LS} &= \mathbf{D}_\mathrm{I}^{+}\hat{\mathbf{u}} \\ &= (\mathbf{D}_\mathrm{I}^\mathrm{H}\mathbf{D})_\mathrm{I}^{-1}\mathbf{D}_\mathrm{I}^\mathrm{H}\hat{\mathbf{u}}. \end{aligned} \tag{10}$$

In general, after solving for $\mathbf{w}_\mathrm{I}$, the final output of the inverse nonlinearity is given as

$$\tilde{\mathbf{u}} = \mathbf{D}_\mathrm{I}\mathbf{w}_\mathrm{I}. \tag{11}$$

This is also the linearized version of the distorted main RX observation $y(n)$, approximating the original baseband-equivalent RX input $u(n)$. Naturally, in the actual online linearization after having estimated the filters $\mathbf{w}_0, \mathbf{w}_1..., \mathbf{w}_\mathrm{P}$ as described above, linearization can be carried out sample by sample without any block-structure.

VI. Linearization Performance Demonstration with RF Measurements

In this section, the performance of the proposed linearization solutions is evaluated and demonstrated with true BS RX hardware and RF measurements. In addition, the performance is compared against previous state-of-the-art. For the single-RX AIC [20] implementation, 100th order digital bandpass

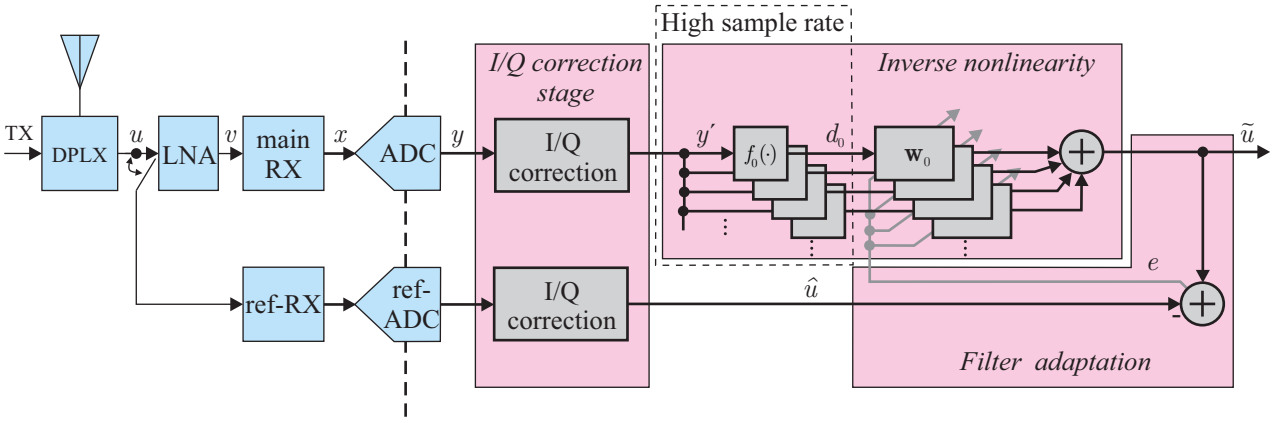

Fig. 4. Block diagram illustrating the principle of the proposed RR-INV method for main RX I/Q correction and linearization. The MFI suppression and nonlinearity inversion stages are cascaded. The I/Q correction stage is implemented based on [36]. The time index n is omitted from the signal notation for illustration convenience.

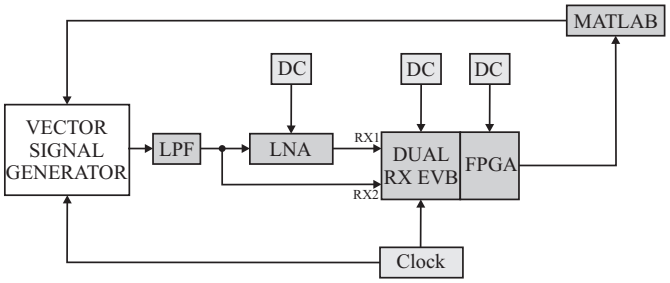

Fig. 5. The measurement setup illustrating device control with Matlab PC and the measurement flow from the vector signal generator to the FPGA connected to the PC.

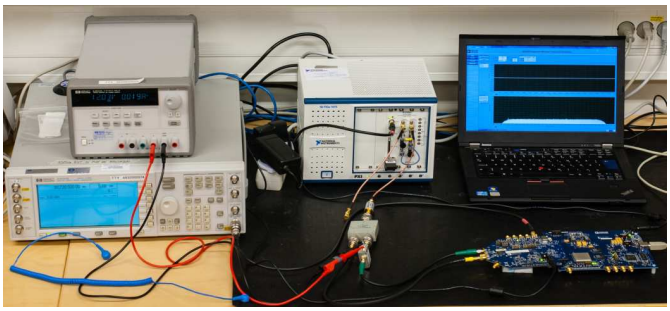

Fig. 6. A photograph of the measurement setup, illustrating the devices used in the laboratory.

and bandstop filters are designed in order to keep the digital front-end complexity realistic. These filters form the bandsplit stage described in [20].

The following measurements replicate two uplink BS multi-carrier reception scenarios [3]. More specifically, 10 MHz 3GPP Long Term Evolution (LTE) uplink single-carrier frequency-division multiple access (SC-FDMA) waveforms with 16-QAM subcarrier modulation are applied. The measured composite signal is generated with National Instruments PXIe-5645R vector signal transceiver. This signal is fed into a splitter, with 3.5 dB attenuation, giving the inputs for the main RX and the ref-RX. In the main RX chain, a HD Communications Cor. HD24089 wideband LNA is employed. The IIP3 and the gain of the LNA are -7 dBm and 22 dB, respectively. After the LNA, a state-of-the-art BS-scale wideband dual-RX board with pre-commercial RX-version of the Analog Devices AD9371 transceiver is used to down-convert, digitize and capture the data. The reception bandwidth of both the RXs is 100 MHz. The measurement set-up is illustrated in more detail in Fig. 5 and shown as a photograph in Fig. 6. For the ref-RX, the received signal is fed without LNA, having thus 22 dB lower RF gain compared to the main RX. The measurements are performed on 1750 MHz RF center frequency.

For the distortion suppression, the following reference nonlinearities and component signals are applied in the RR-AIC

$$\begin{aligned} d_0(n) &= f_0(\hat{u}(n)) = \hat{u}(n), \\ d_1(n) &= f_1(\hat{u}(n)) = \hat{u}^2(n), \\ d_2(n) &= f_2(\hat{u}(n)) = [\hat{u}^*(n)]^2, \\ d_3(n) &= f_3(\hat{u}(n)) = |\hat{u}(n)|^2, \\ d_4(n) &= f_4(\hat{u}(n)) = |\hat{u}(n)|^2\hat{u}(n), \\ d_5(n) &= f_5(\hat{u}(n)) = [\hat{u}^*(n)]^3, \\ d_6(n) &= f_6(\hat{u}(n)) = |\hat{u}(n)|^4\hat{u}(n), \end{aligned} \tag{12}$$

where the second, third and fifth order nonlinearities are considered for optimizing linearization performance. In the RR-INV processing, the same reference nonlinearities $f_0(\cdot), f_1(\cdot), ..., f_6(\cdot)$ are applied for the received and I/Q corrected main RX signal $y'(n)$, instead of $\hat{u}(n)$ used in (12), as illustrated in Fig. 4. These distortion components from Table I have been chosen based on trials in the RF measurements with the utilized RX hardware. The significance of these components is further studied and demonstrated in Sub-Section VI-C. Two-tap adaptive filters, per nonlinear basis function, are applied in both the RR-AIC and RR-INV linearization stages in order to consider mild memory effects. Furthermore, two-tap filters are also adopted in the I/Q correction stages, building on [36]. This, as well, allows considering mild frequency selectivity in the I/Q mismatch appearing in the measurement setup. The signal-to-noise-and-distortion ratio (SNDR) and uncoded symbol error ratio (SER) results are obtained using the block LS based parameter learning. These figures of merit are evaluated and averaged over 10 independent measurements each consisting of 305 600

TABLE II
SIGNAL AND MAJOR DISTORTION COMPONENTS IN NON-OVERLAPPING NONLINEAR DISTORTION AND MIRROR-FREQUENCY INTERFERENCE SCENARIO. THE SHOWN CENTER FREQUENCIES REFER TO THE IQ DOWN-CONVERTER OUTPUT.

Component	Center Freq.	BW	Power
Weak carrier 1	-40 MHz	10 MHz	-77 dBm (RF)
Weak carrier 2	20 MHz	10 MHz	-77 dBm (RF)
Blocker 1	10 MHz	10 MHz	swept
Blocker 2	40 MHz	10 MHz	swept
Mirror Term 1	-10 MHz	10 MHz	varies
Mirror Term 2	-40 MHz	10 MHz	varies
3rd Ord. Spreading 1	10 MHz	30 MHz	varies
3rd Ord. Spreading 2	40 MHz	30 MHz	varies
3rd Ord. Intermodulation	-20 MHz	30 MHz	varies

complex-valued received samples. When sweeping the blocker power in the measurements, the power step for each blocker is 2 dB.

A. Suppression Quantification for Non-overlapping Nonlinear Distortion and Mirror-frequency Interference

In this scenario, two weak LTE uplink carriers are received in the presence of two strong blocking carriers. The weak carriers are placed in such a manner that the other one suffers from the MFI and the other one from the nonlinear distortion induced by the strong carriers. The details of this signal scenario are gathered in Table II.

Snapshot spectral examples are shown in Fig. 7 in order to illustrate the signal scenario and the major performance differences between the solutions. The strong blocking carriers, responsible for the dominating distortion components in the black spectra of the original received signal, are located after the RF I/Q down-conversion at the IF center frequencies of 10 MHz and 40 MHz. The strongest distortion components appear thus on the mirror bands, around the original strong carriers, with triple bandwidth typical for 3rd-order IMD, and around -20 MHz (2×10 MHz $-$ 40 MHz $=-20$ MHz, 3rd-order IMD). The weak LTE carriers are in this example located at the IF center frequencies of -40 MHz and 20 MHz. Thus, MFI stemming from the strong carrier located at 40 MHz and 3rd-order IMD due to the other strong carrier at 10 MHz are falling on top of these weak carriers, respectively.

In Fig. 7, it can be observed that the earlier proposed AIC processing without ref-RX [20] is suppressing the IMD spread around the strong carriers poorly compared to the proposed ref-RX enhanced approaches. Also 3rd-order IMD around -20 MHz remains at slightly higher level compared to the proposed RR-AIC and RR-INV. However, all three solutions show clearly improved signal quality at the mirror bands of the strong carriers which is best illustrated around -10 MHz signal band, where the image of the 10 MHz carrier can be seen without underlying weak carrier.

Furthermore, Fig. 8 shows the SNDRs for both the weak signals (around -40 MHz and 20 MHz) with different linearization solutions as a function of the blocker power at the splitter input preceding the main RX LNA. The solid lines in Fig. 8 show good improvement in the -40 MHz weak carrier SNDR. For example at the 14 dB SNDR level, 21 dB stronger mirror-band blocker is tolerated compared to the original received scenario. As an example, at -27 dBm blocker RF power level, the SNDR of the mirror-band weak carrier is increased from -1 dB to 15 dB with all the studied solutions. Considering the weak carrier around -40 MHz, it should be noted that most of the SNDR gain is achieved by the MFI suppression.

The dashed lines show then the SNDRs for the 20 MHz weak carrier located close to the 10 MHz strong carrier. The

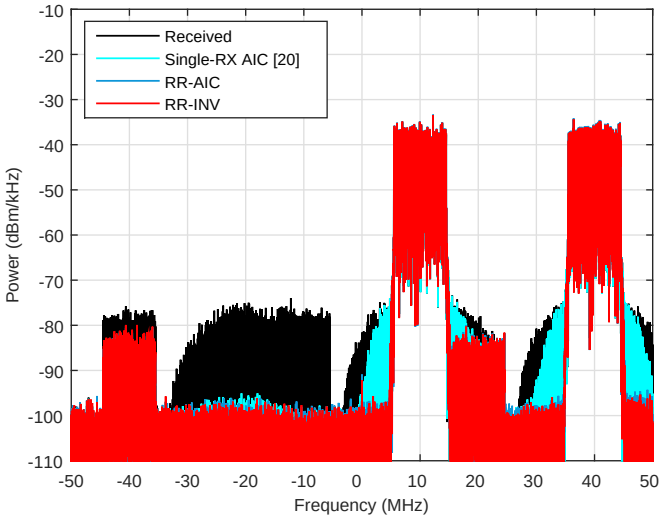

Fig. 7. The measured spectra of the original received and the linearized signals at digital BB/IF, illustrating the performance of the RR-AIC and RR-INV. The blocker powers are -23 dBm and weak carrier powers are -77 dBm per carrier, when evaluated at the RX input at RF. The weak carriers are located at 20 MHz and -40 MHz.

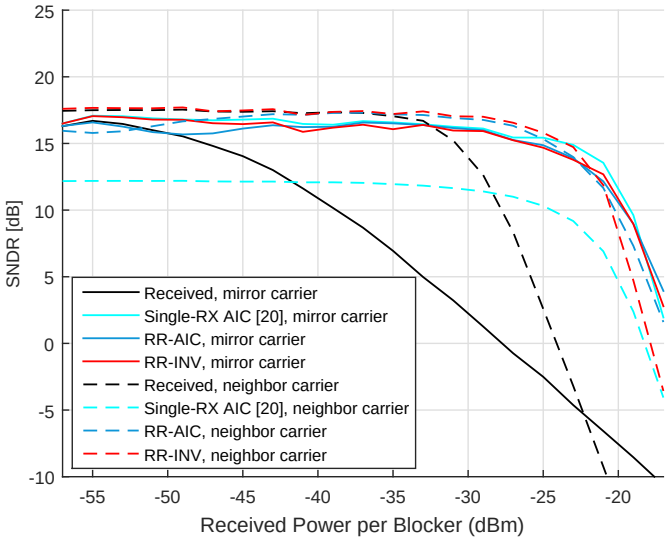

Fig. 8. The measured SNDRs of the mirror-band weak carrier around -40 MHz ("mirror carrier") and the neighboring-band weak carrier around 20 MHz ("neighbor carrier") as functions of the blocker RF powers. The mirror carrier and neighbor carrier SNDRs are presented with solid and dashed lines, respectively. The weak carrier RF powers are constant -77 dBm per carrier.

black dashed line shows that at this band the SNDR starts to suffer only at the higher blocker powers, which is typical for nonlinearity dominated distortion profile. As can be observed in Fig. 7, the single-RX AIC [20] is performing poorly compared to the proposed ref-RX solutions. Between the RR-AIC and RR-INV, the RR-INV is slightly outperforming RR-AIC on most of the practical reception quality range. With the very highest blocker RF powers studied, the RR-AIC gives 2–4 dB higher SNDR compared to RR-INV. Up to the $-27\,\mathrm{dBm}$ RF blocker power specified by 3GPP as one test scenario [3], the performance is practically equal. Again, at the 14 dB SNDR level, the blocker tolerance compared to no linearization at all is improved from the 20 MHz weak carrier point-of-view by 7.0 dB with RR-AIC and 7.5 dB with RR-INV. At the same time, at $-27\,\mathrm{dBm}$ blocker power level, the SNDR of the neighboring band weak carrier is increased from 8 dB to 11 dB and 16 dB with the single-RX AIC and both the ref-RX solutions, respectively. Overall, Fig. 8 shows that similar levels of post-linearization SNDRs can be achieved for both weak carriers, independent of the differences in pre-linearization SNDR levels.

In Fig. 9, the uncoded SER results for mirror band and neighboring band carriers follow generally the same trends as observed for the SNDRs. For the mirror band carrier, 1% uncoded SER levels are maintained with 20–22 dB higher blocker powers compared to the original received signal without post-processing. At the same time, for example at the $-27\,\mathrm{dBm}$ blocker power level the uncoded SER is improved from 80% to below 1%. For the neighboring carrier, the single-RX AIC [20] performance is poor also when measured with SER. In parallel, the RR-AIC and RR-INV allow 6 dB blocker tolerance improvement at 1% uncoded SER level. Also in this case, SER in $-27\,\mathrm{dBm}$ blocker case is pushed below 1% when uncompensated SER is 27%.

Generally, the results clearly show that the proposed solutions outperform the existing state-of-the-art [20], in particular when considering the linearization performance at frequencies close to the strong carriers.

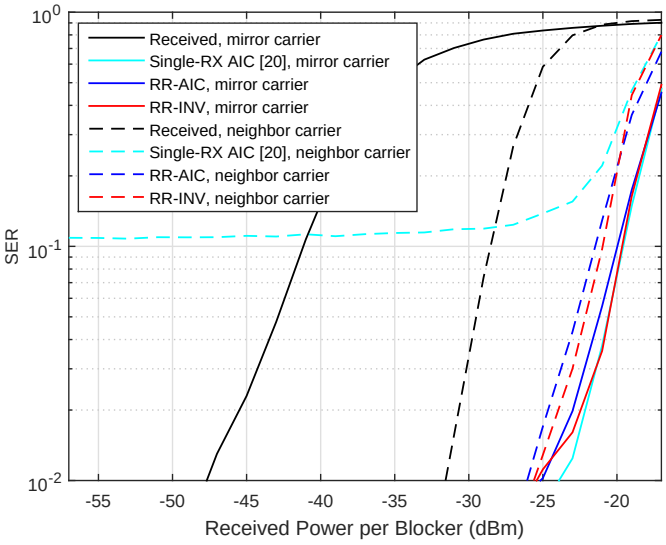

Fig. 9. The measured SERs of the mirror-band weak carrier around -40 MHz ("mirror carrier") and the neighboring-band weak carrier around 20 MHz ("neighbor carrier") as functions of the blocker RF powers. The mirror carrier and neighbor carrier SNDRs are presented with solid and dashed lines, respectively. The weak carrier RF powers are constant $-77\,\mathrm{dBm}$ per carrier.

TABLE III
SIGNAL AND MAJOR DISTORTION COMPONENTS IN OVERLAPPING NONLINEAR DISTORTION AND MIRROR-FREQUENCY INTERFERENCE SCENARIO. THE SHOWN CENTER FREQUENCIES REFER TO THE IQ DOWN-CONVERTER OUTPUT.

Component	Center Freq.	BW	Power
Weak carrier	-10 MHz	10 MHz	$-77\,\mathrm{dBm}$ (RF)
Blocker 1	10 MHz	10 MHz	swept
Blocker 2	30 MHz	10 MHz	swept
Mirror Term 1	-10 MHz	10 MHz	varies
Mirror Term 2	-30 MHz	10 MHz	varies
3rd Ord. Spreading 1	10 MHz	30 MHz	varies
3rd Ord. Spreading 2	30 MHz	30 MHz	varies
3rd Ord. Intermodulation	-10 MHz	30 MHz	varies

B. Suppression Quantification for Overlapping Nonlinear Distortion and Mirror-frequency Interference

In this scenario, a single weak carrier is received in the presence of two blocking carriers such that the MFI and the nonlinear distortion are all falling on the same band together with the weak carrier. From the weak carrier point-of-view, this can be considered as a worst-case scenario. The details of this signal scenario are gathered in Table III.

In Fig. 10, spectral examples in case of a weak LTE carrier masked by overlapping MFI and 3rd-order IMD are illustrated. The overall distortion profile differs in this scenario from that of the previous subsection because the strong blocking carriers are now located at IF center frequencies of 10 MHz and 30 MHz instead of 10 MHz and 40 MHz that were adopted in the previous scenario. The weak carrier, in turn, is situated around IF center frequency of -10 MHz. From the linearization performance point-of-view, it is again clearly visible in Fig. 10 that the AIC with main RX only processing [20] suffers from poor performance at the frequencies close to the strong carriers. Otherwise, the performance of all the studied solutions is close to each other in this snapshot example. It should be again noted, that the MFI due to the 30 MHz strong carrier falling to around -30 MHz is pushed down to the noise level, which points toward good MFI suppression performance also at the weak carrier band around -10 MHz, where the MFI of the 10 MHz strong carrier is present. Also the IMD around the weak carrier band seems to be efficiently pushed down.

The actual SNDR of the weak carrier is evaluated and illustrated in Fig. 11 in order to achieve concrete insight on the distortion levels inside this band. Generally, in Fig. 11, it is visible that the RR-INV gives most solid SNDR performance over the whole measured range. All the compared solutions are, generally speaking, achieving significant improvement in the weak carrier signal quality. For example, at the previously

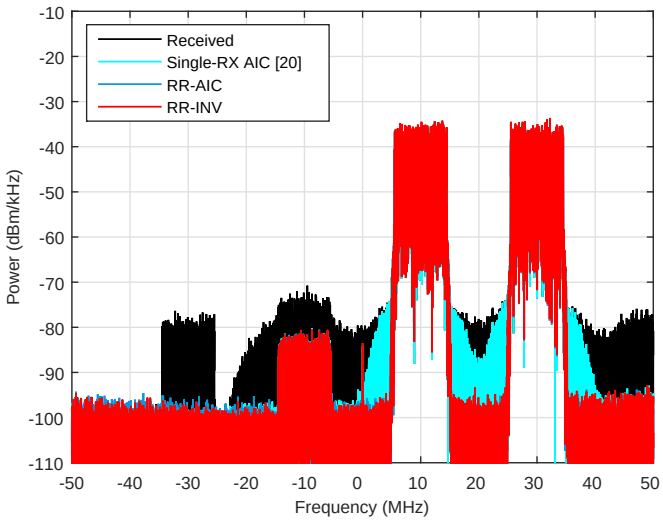

Fig. 10. The measured spectra of the original received and the linearized signals at digital BB/IF, illustrating the performance of the RR-AIC and RR-INV in the weak carrier worst-case scenario. The blocker powers are $-23\,\mathrm{dBm}$ and weak carrier power is $-77\,\mathrm{dBm}$, when evaluated at the RX input at RF. The weak carrier is located at $-10\,\mathrm{MHz}$.

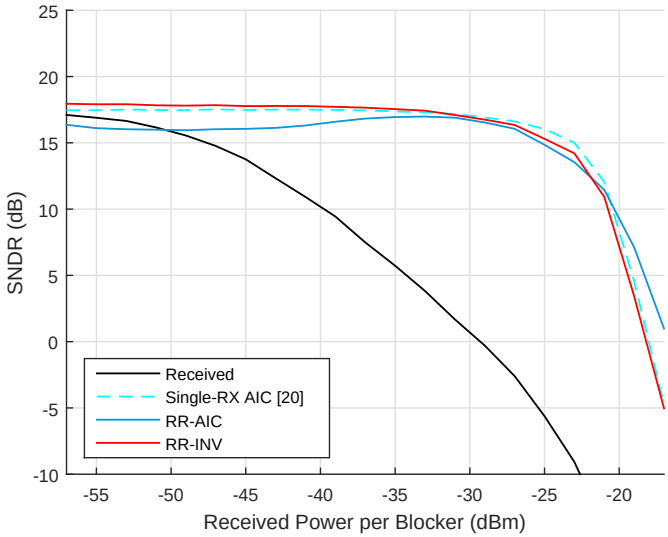

Fig. 11. The measured SNDR of the worst-case weak carrier (around $-10\,\mathrm{MHz}$) as a function of the blocker RF powers. The weak carrier RF power is constant $-77\,\mathrm{dBm}$.

mentioned target SNDR level of $14\,\mathrm{dB}$, the RR-INV improves blocker tolerance of the RX, compared to no linearization, by $23\,\mathrm{dB}$ and the other two solutions lie within $1\,\mathrm{dB}$ interval. Furthermore, $16\,\mathrm{dB}$ post-linearization SNDR is achieved by all the studied solutions at the blocker power levels of $-27\,\mathrm{dBm}$ while the pre-linearization SNDR is approximately $-3\,\mathrm{dB}$, demonstrating thus a significant gain of $19\,\mathrm{dB}$. It should be noted that this $19\,\mathrm{dB}$ gain consists of the combined MFI suppression and linearization performance that can be achieved with these solutions.

In Fig. 12, the SERs are shown for the weak carrier. The uncoded SER performance of the single-RX AIC [20] and the RR-INV are close to each other while the RR-AIC performs poorer with the low blocker powers. Considering again 1% uncoded SER level, the single-RX AIC [20] and the RR-INV

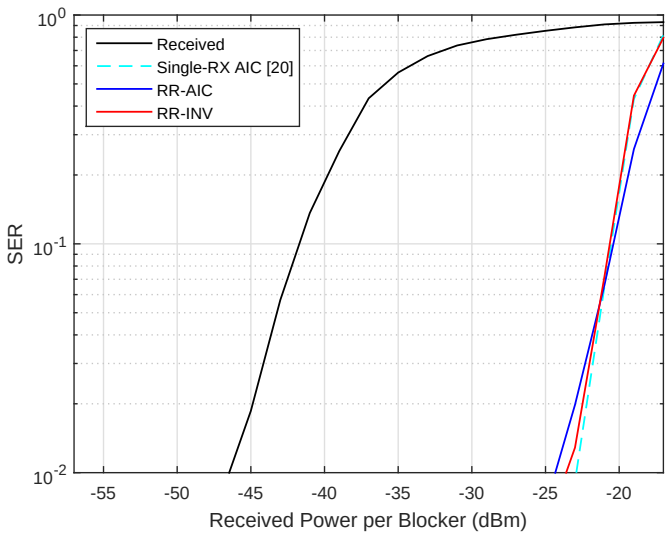

Fig. 12. The measured uncoded SER of the worst-case weak carrier (around $-10\,\mathrm{MHz}$) as a function of the blocker RF powers. The weak carrier RF power is constant $-77\,\mathrm{dBm}$.

offer $23\,\mathrm{dB}$ improvement in the blocker tolerance, the RR-AIC being also very close at $22\,\mathrm{dB}$. With the $-27\,\mathrm{dBm}$ blocker power, all the solutions push the SER level from 82% below 1% level. In this scenario, the single-RX AIC [20] achieves marginal edge over RR-AIC and RR-INV by dropping below 1% SER level with $1\,\mathrm{dB}$ higher blocker powers.

Overall, the RR-AIC falls below the RR-INV and the single-RX AIC with the lower blocking carrier power levels and with lowest power levels is actually slightly decreasing the SNDR level compared to the original received signal. This kind of behavior has been documented with such cancellation algorithms also earlier [25]. However, if, for example, pilot-based estimation of the signal quality indicates good reception conditions, the linearization processing can and should be switched off in order to save processing power, at the same time avoiding these effects.

C. Linearization Performance with Different Reference Nonlinearity Subsets

In Fig. 13, the role of chosen reference nonlinearities, given in (12), is illustrated using RR-INV linearization and $-23\,\mathrm{dBm}$ blocker powers as a concrete example. Furthermore, the weak carrier worst case scenario discussed in Sub-Section VI-B and detailed in Table III is used. In the figure, it is visible that including $d_4(n)$ and $d_6(n)$ has the biggest effect on the linearization performance. This indicates that with the given hardware, the third- and fifth-order intermodulations are the dominant distortion components. This is further demonstrated in Table IV, where examples of the weak carrier SNDR and uncoded SER are given. Herein, also second-order components and third-order harmonic component in (12) are included in the processing in order to maximize the overall performance on the whole reception band. If lower-complexity solution is desired, reduced set of reference nonlinearities can be considered. For example, in addition to linear Term $d_0(n)$, solely third- and fifth-order intermodulation Terms $d_4(n)$ and

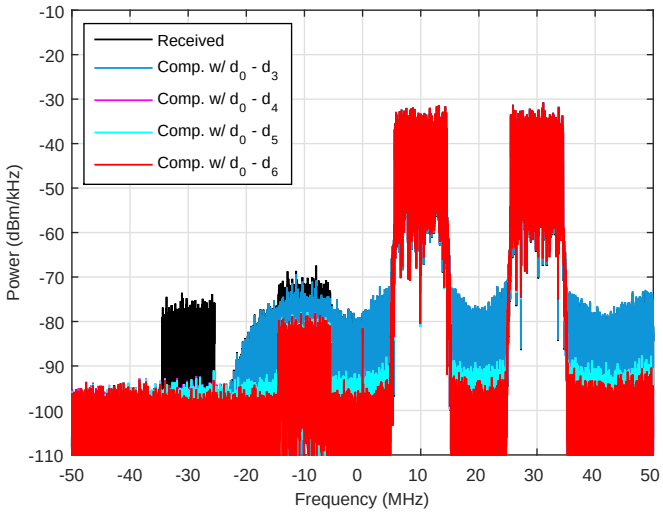

Fig. 13. The measured spectra of the original received and the linearized signals at digital BB/IF, illustrating the role of the applied reference nonlinearities, given in (12). The blocker powers are $-23\,\mathrm{dBm}$ and weak carrier power is $-77\,\mathrm{dBm}$, when evaluated at the RX input at RF.

TABLE IV
SNDR AND UNCODED SER OF THE WEAK CARRIER WITH VARIED RR-INV REFERENCE NONLINEARITY SUBSETS AND $-23\,\mathrm{dBm}$ BLOCKER POWERS IN OVERLAPPING NONLINEAR DISTORTION AND MIRROR-FREQUENCY INTERFERENCE SCENARIO.

Components	Weak Carrier SNDR	Weak Carrier SER
Uncompensated	$-8.8\,\mathrm{dB}$	88%
$d_0, ..., d_3$	$-6.0\,\mathrm{dB}$	84%
$d_0, ..., d_4$	$11\,\mathrm{dB}$	7.1%
$d_0, ..., d_5$	$11\,\mathrm{dB}$	7.2%
$d_0, ..., d_6$	$15\,\mathrm{dB}$	1.1%

$d_6(n)$ could be employed. On the other hand, if the hardware at hand contained even stronger BB nonlinearity, the contribution of the second-order Terms $d_1(n), d_2(n)$ and $d_3(n)$ and the third-order harmonic Term $d_5(n)$ would increase, because they are tackling exactly this BB distortion. Also cascaded effects of the RF and BB nonlinearities are covered by the Terms in Table I based on the modeling in (1)–(3). Furthermore, it should be noted, as mentioned in Section III, that $d_4(n)$ and $d_6(n)$ are induced both by the RF nonlinearity and the BB nonlinearity. The exact choice of Terms is thus highly hardware-dependent and exact universal guidelines do not exist, as discussed in Section IV-A. Altogether, the provided RF measurement results successfully demonstrate and verify the good linearization performance of the proposed solutions.

VII. FURTHER DISCUSSION

The main benefit of the proposed linearization solutions is the improved distortion suppression performance, as demonstrated in Section VI. However, the ref-RX approach brings also additional advantages compared to previous solutions. These are shortly discussed below.

Compared to, e.g., [20], no digital bandpass or bandstop filters are needed for separating the strongest distortion inducing carriers and removing the blocker inband contribution from the distortion estimate, respectively. This simplifies implementation of the digital front-end significantly. Especially because, as noted in Section VI, the response of these filters directly affects the linearization performance of the single-RX version of the AIC. Thus, very high order filters would be needed if the linearization performance should be optimized.

Another advantage stemming from the fact that the above-mentioned digital front-end filters can be avoided is that no exact information of the strongest blocking carrier center frequencies and bandwidths is needed in the RR-AIC and the RR-INV. The whole main RX observation is processed as is without need for bandsplit or other filtering stages, or spectrum sensing for the strongest carriers [20], [21], simplifying the digital front-end processing significantly.

The cost of the proposed linearization solutions is the implementation and power consumption of the ref-RX together with the the digital correction logic proposed herein. It is still an open question if the current RX systems can tolerate this overhead. However, obtaining accurate power consumption estimates would require implementation on silicon, and even in such approach, the results would be highly case and process dependent. On the other hand, power consumption estimation based on the amount of operations results commonly in inaccurate and highly speculative results, and was therefore not included in this paper. Thus, more detailed complexity and power consumption analyses and optimization in different wideband RX scenarios, e.g., in the context of cellular networks, are left for future work. Potential complexity reduction techniques for the linearization DSP have been proposed, especially in the context of the transmitter DPD [40], [41]. They could potentially be applied for the digital RX linearization for reducing the power consumption of the related DSP, as the cost of the DSP should not be ignored. On the analog side, in general, the ref-RX performance metrics are quite different to the main RX, which is designed for worst-case situation seeking to optimize the challenging combination of linearity, sensitivity and dynamic range. The ref-RX, in turn, only needs to observe the strong signals and thus, e.g., the sensitivity requirements are substantially reduced, leading to simplified and lower-cost implementation prospects. At the same time, the integrability of the DCR allows also dual-RX chips making efficient implementation of the ref-RX and data transfer to the BB processing unit possible.

Based on the results presented in Section VI, the proposed RR-INV solution gives the best overall performance in the studied scenarios. Therein, blocker tolerance improvement of $23\,\mathrm{dB}$ and weak carrier SNDR gain of $19\,\mathrm{dB}$ together with uncoded SER improvement from 82% to below 1% were demonstrated in the considered worst-case distortion scenario with combined suppression of the MFI and the nonlinear distortion. In addition, because in RR-INV no cancellation signal that should be continuously available is produced from the ref-RX received signal, it is possible to run the calibration of the inverse nonlinearity only periodically. This would allow decreased power consumption because of the turned-off ref-RX analog components, such as amplifiers and ADCs as well as the digital parameter learning algorithms. In addition,

in multi-antenna RX scenarios with multiple parallel DCR chains, this opens up potential for linearization and parameter learning such that only one ref-RX, shared sequentially between the main RXs, is adopted. In such scenarios, the hardware overhead of the adoption of the ref-RX is thus already minimal. Thus, RR-INV is a very potential candidate for linearizing cellular BS RXs, where wideband multi-operator, multi-technology, multi-carrier reception is a desirable feature, leading to the aforementioned challenges with very high inband and out-of-band blocker tolerance requirements.

VIII. Conclusion

In this paper, an arbitrary order parallel Hammerstein model for wideband DCRs was first developed to characterize the overall RX nonlinear behavior. The model incorporates the effects of both RF and BB nonlinearities and I/Q mismatch of the down-conversion mixers and BB I and Q components. The results of this modeling were then applied in developing two novel digital post-linearization solutions for suppressing the nonlinear distortion introduced both at the RF and at the BB stages of the RX front-end, building on the concept of adopting a ref-RX to observe the incoming signal with reduced sensitivity but enhanced linearity. The proposed RR-AIC adaptively finds the parameters of the nonlinearity model of the front-end and provides distortion signal estimate for cancellation. The proposed RR-INV, in turn, finds the inverse nonlinearity model which minimizes the distortion power at the output of the inverse nonlinearity when the whole received signal is fed as an input. Both of these solutions can offer improved performance over the state-of-the-art at a cost of a single additional DCR chain while also resulting to substantially simplified digital front-end signal processing.

As the actual cost of an additional integrated RX chain is already pushed down with modern CMOS processes, the RR-AIC and especially the RR-INV offer attractive options for linearizing cellular wideband multi-operator, multi-technology, multi-carrier BS RXs. In this way, need for expensive high-performance, high-cost analog components can potentially be relaxed and the complexity can be moved towards digital domain, where the computation power is becoming more and more cost-effective.

References

[1] *Digital cellular telecommunications system (Phase 2+); Radio transmission and reception*, 3GPP TS 45.005 version 11.4.0 Release 11, Jan. 2014.

[2] *Universal Mobile Telecommunications System (UMTS); Base Station (BS) radio transmission and reception (FDD)*, 3GPP TS 25.104 version 11.8.0 Release 11, Jan. 2014.

[3] *LTE; Evolved Universal Terrestrial Radio Access (E-UTRA); Base Station (BS) radio transmission and reception*, 3GPP TS 36.104 version 11.7.0 Release 11, Jan. 2014.

[4] A. Gupta and R. Jha, "A survey of 5G network: Architecture and emerging technologies," *IEEE Access*, vol. 3, pp. 1206–1232, 2015.

[5] B. Razavi, "Design considerations for direct-conversion receivers," *IEEE Trans. Circuits Syst. II*, vol. 44, no. 6, pp. 428–435, June 1997.

[6] ——, "Cognitive radio design challenges and techniques," *IEEE J. Solid-State Circuits*, vol. 45, no. 8, pp. 1542–1553, Aug. 2010.

[7] D. H. Mahrof, E. A. M. Klumperink, J. C. Haartsen, and B. Nauta, "On the effect of spectral location of interferers on linearity requirements for wideband cognitive radio receivers," in *Proc. IEEE Symp. on New Frontiers in Dynamic Spectrum*, Singapore, Apr. 2010, pp. 1–9.

[8] L. Anttila, "Digital front-end signal processing with widely-linear signal models in radio devices," Ph.D. dissertation, Tampere University of Technology, Finland, 2011. [Online]. Available: http://urn.fi/URN:ISBN:978-952-15-2978-8

[9] A. Shahed Hagh Ghadam, "Contributions to analysis and DSP-based mitigation of nonlinear distortion in radio transceivers," Ph.D. dissertation, Tampere University of Technology, Finland, 2011. [Online]. Available: http://urn.fi/URN:ISBN:978-952-15-2794-4

[10] M. Allén, "Nonlinear distortion in wideband radio receivers and analog-to-digital converters: Modeling and digital suppression," Ph.D. dissertation, Tampere University of Technology, Finland, 2015. [Online]. Available: http://urn.fi/URN:ISBN:978-952-15-3611-3

[11] G. Fettweis, M. Lohning, D. Petrovic, M. Windisch, P. Zillmann, and W. Rave, "Dirty RF: a new paradigm," in *Proc. 16th Annual IEEE International Symposium on Personal, Indoor and Mobile Radio Communications*, Berlin, Germany, 11-14 Sept. 2005, pp. 2347–2355.

[12] E. Keehr and A. Hajimiri, "Equalization of third-order intermodulation products in wideband direct conversion receivers," *IEEE J. Solid-State Circuits*, vol. 43, no. 12, pp. 2853–2867, Dec. 2008.

[13] Q. Zou, M. Mikhemar, and A. H. Sayed, "Digital compensation of cross-modulation distortion in software-defined radios," *IEEE J. Sel. Topics Signal Process.*, vol. 3, pp. 348–361, June 2009.

[14] A. A. Abidi, "Direct-conversion radio transceivers for digital communications," *IEEE J. Solid-State Circuits*, vol. 30, no. 12, pp. 1399–1410, Dec. 1995.

[15] E. Keehr and A. Hajimiri, "Successive regeneration and adaptive cancellation of higher order intermodulation products in RF receivers," *IEEE Trans. Microw. Theory Techn.*, vol. 59, no. 5, pp. 1379–1396, May 2011.

[16] A. Shahed Hagh Ghadam, M. Valkama, and M. Renfors, "Adaptive compensation of nonlinear distortion in multicarrier direct-conversion receivers," in *Proc. IEEE Radio and Wireless Conference*, Sept 2004, pp. 35–38.

[17] M. Valkama, A. Shahed Hagh Ghadam, L. Anttila, and M. Renfors, "Advanced digital signal processing techniques for compensation of nonlinear distortion in wideband multicarrier radio receivers," *IEEE Trans. Microw. Theory Techn.*, vol. 54, no. 6, pp. 2356–2366, June 2006.

[18] M. Allén, J. Marttila, and M. Valkama, "Modeling and mitigation of nonlinear distortion in wideband A/D converters for cognitive radio receivers," *European Microwave Assoc. Int. J. Microwave and Wireless Technologies*, vol. 20, pp. 183–192, Apr. 2010.

[19] M. Allén, J. Marttila, M. Valkama, S. Mäkinen, M. Kosunen, and J. Ryynänen, "Digital linearization of direct-conversion spectrum sensing receiver," in *Proc. 1st IEEE Global Conf. Signal and Information Process.*, Austin, TX, USA, Dec. 2013, pp. 1158–1161.

[20] M. Grimm, M. Allén, J. Marttila, M. Valkama, and R. Thomä, "Joint mitigation of nonlinear RF and baseband distortions in wideband direct-conversion receivers," *IEEE Trans. Microw. Theory Techn.*, vol. 62, no. 1, pp. 166–182, Jan. 2014.

[21] E. Rebeiz, A. Ghadam, M. Valkama, and D. Cabric, "Spectrum sensing under rf non-linearities: Performance analysis and dsp-enhanced receivers," *IEEE Transactions on Signal Processing*, vol. 63, no. 8, pp. 1950–1964, April 2015.

[22] M. Allén and J. Marttila and M. Valkama and S. Singh and M. Epp and W. Schlecker, "Digital full-band linearization of wideband direct-conversion receiver for radar and communications applications," in *Proc. 49th Asilomar Conference on Signals, Systems and Computers*, Pacific Grove, CA, Nov. 2015, pp. 1361–1368.

[23] K. Dogancay, "Blind compensation of nonlinear distortion for bandlimited signals," *IEEE Trans. Circuits Syst. I, Reg. Papers*, vol. 52, no. 9, pp. 1872–1882, Sept 2005.

[24] M. Allén, J. Marttila, and M. Valkama, "Digitally-enhanced wideband analog-digital interfaces for future cognitive radio devices," in *Proc. 8th IEEE Int. NEWCAS Conf.*, Montreal, Canada, June 2010, pp. 361–364.

[25] M. Allén, J. Marttila, M. Valkama, M. Grimm, and R. Thoma, "Digital post-processing based wideband receiver linearization for enhanced spectrum sensing and access," in *9th Int. Conf. Cognitive Radio Oriented Wireless Networks and Commun.*, Oulu, Finland, June 2014, pp. 520–525.

[26] D. Stepanovic and B. Nikolic, "A 2.8 GS/s 44.6 mW time-interleaved ADC achieving 50.9 dB SNDR and 3 dB effective resolution bandwidth of 1.5 GHz in 65 nm CMOS," *IEEE J. Solid-State Circuits*, vol. 48, no. 4, pp. 971–982, April 2013.

[27] F. M. Ghannouchi and O. Hammi, "Behavioral modeling and predistortion," *IEEE Microwave Magazine*, vol. 10, no. 7, pp. 52–64, Dec 2009.

[28] J. Zhou and A. Chakrabarti and P. R. Kinget and H. Krishnaswamy, "Low-Noise Active Cancellation of Transmitter Leakage and Transmitter

Noise in Broadband Wireless Receivers for FDD/Co-Existence," *IEEE J. Solid-State Circuits*, vol. 49, no. 12, pp. 3046–3062, Dec. 2014.
[29] T. Zhang and A. R. Suvarna and V. Bhagavatula and J. C. Rudell, "An Integrated CMOS Passive Self-Interference Mitigation Technique for FDD Radios," *IEEE J. Solid-State Circuits*, vol. 50, no. 5, pp. 1176–1188, May 2015.
[30] A. Kiayani and L. Anttila and M. Valkama, "Digital Suppression of Power Amplifier Spurious Emissions at Receiver Band in FDD Transceivers," *IEEE Signal Process. Lett.*, vol. 21, no. 1, pp. 69–73, Jan. 2014.
[31] A. Kiayani and M. Abdelaziz and L. Anttila and V. Lehtinen and M. Valkama, "Digital Mitigation of Transmitter-Induced Receiver Desensitization in Carrier Aggregation FDD Transceivers," *IEEE Trans. Microw. Theory Techn.*, vol. 63, no. 11, pp. 3608–3623, Nov. 2015.
[32] P. Landin, "On radio frequency behavioral modeling," Licensiate thesis, Royal Institute of Technology (KTH), 2009. [Online]. Available: http://www.diva-portal.org/smash/get/diva2:279216/FULLTEXT01.pdf
[33] ——, "Digital baseband modeling and correction of radio frequency power amplifiers," Ph.D. dissertation, Royal Institute of Technology (KTH), 2012. [Online]. Available: http://www.diva-portal.org/smash/get/diva2:526062/SPIKBLAD.pdf
[34] H. Gutierrez, K. Gard, and M. Steer, "Nonlinear gain compression in microwave amplifiers using generalized power-series analysis and transformation of input statistics," *IEEE Transactions on Microwave Theory and Techniques*, vol. 48, no. 10, pp. 1774–1777, Oct 2000.
[35] P. B. Kenington, *High-Linearity RF Amplifier Design*. Norwood, MA: Artech House, 2000, pp. 74–77.
[36] L. Anttila, M. Valkama, and M. Renfors, "Circularity based I/Q imbalance compensation in wideband direct-conversion receivers," *IEEE Trans. Veh. Technol.*, vol. 57, no. 4, pp. 2099–2113, July 2008.
[37] E. Bautista and B. Bastani and J. Heck, "Improved mixer IIP2 through dynamic matching," in *Digest of Technical Papers IEEE Int. Solid-State Circuits Conference*, San Fransisco, CA, Feb. 2000, pp. 376–377.
[38] S. Haykin, *Adaptive Filter Theory*, 4th ed. Upper Saddle river, NJ: Prentice Hall, 2002.
[39] J. Tsimbinos and K. V. Lever, "Nonlinear system compensation based on orthogonal polynomial inverses," *IEEE Transactions on Circuits and Systems: Fundamental Theory and Applications*, vol. 48, no. 4, pp. 406–417, Apr 2001.
[40] L. Guan and A. Zhu, "Low-Cost FPGA Implementation of Volterra Series-Based Digital Predistorter for RF Power Amplifiers," *EEE Trans. Microw. Theory Techn.*, vol. 58, no. 4, pp. 866–872, April 2010.
[41] P. L. Gilabert and G. Montoro and D. López and N. Bartzoudis and E. Bertran and M. Payaró and A. Hourtane, "Order reduction of wideband digital predistorters using principal component analysis," in *IEEE MTT-S Int. Microwave Symp. Digest*, Seattle, WA, June 2013, pp. 1–7.

Jaakko Marttila (S'10) was born in Tampere, Finland, on March 30, 1982. He received the M.Sc. and D.Sc. degrees in signal processing and communications engineering from Tampere University of Technology (TUT), Tampere, Finland, in 2010 and 2014, respectively.

He is currently working as a Post-Doctoral Researcher at TUT, Department of Electronics and Communications Engineering. His research interests are digital compensation of radio receiver nonidealities and analog-to-digital (AD) conversion techniques for software defined and cognitive radios.

Markus Allén (S'10) was born in Ypäjä, Finland, on October 28, 1985. He received the B.Sc., M.Sc. and D.Sc. degrees in signal processing and communications engineering from Tampere University of Technology, Finland, in 2008, 2010 and 2015, respectively.

He is currently with the Department of Electronics and Communications Engineering at Tampere University of Technology as a University Teacher. His current research interests include cognitive radios, analog-to-digital converters, receiver front-end nonlinearities and their digital mitigation algorithms.

Marko Kosunen (S'97-M'07) received his M.Sc, L.Sc and D.Sc (with honors) degrees from Helsinki University of Technology, Espoo, Finland, in 1998, 2001 and 2006, respectively.

He is currently a Senior Researcher at Aalto University, Department of Micro and Nanosciences. His expertise is in implementation of the wireless transceiver DSP algorithms and communication circuits. He is currently working on implementations of cognitive radio spectrum sensors, digital intensive transceiver circuits and medical sensor electronics.

Kari Stadius (S'95–M'03) received the M.Sc., Lic. Tech., and D.Sc. degrees in electrical engineering from the Helsinki University of Technology, Helsinki, Finland, in 1994, 1997, and 2010, respectively.

He is currently working as a Staff Scientist at the Department of Micro- and Nanosciences, Aalto University School of Electrical Engineering. His research interests include the design and analysis of RF transceiver blocks with special emphasis on frequency synthesis.

Jussi Ryynänen (S'99-M'04) was born in Ilmajoki, Finland, in 1973. He received his Master of Science, Licentiate of Science, and Doctor of Science degrees in electrical engineering from Helsinki University of Technology (HUT), Helsinki, Finland, in 1998, 2001, and 2004, respectively.

He is currently working as an associate professor at the Department of Micro- and Nanosciences, Aalto University School of Electrical Engineering. His main research interests are integrated transceiver circuits for wireless applications. He has authored or coauthored over 100 refereed journal and conference papers in the areas of analog and RF circuit design. He holds six patents on RF circuits

Mikko Valkama (S'00, M'02) was born in Pirkkala, Finland, on November 27, 1975. He received the M.Sc. and Ph.D. degrees (both with honours) in electrical engineering (EE) from Tampere University of Technology (TUT), Finland, in 2000 and 2001, respectively. In 2002 he received the Best Ph.D. Thesis award by the Finnish Academy of Science and Letters for his dissertation entitled "Advanced I/Q signal processing for wideband receivers: Models and algorithms".

In 2003, he was working as a visiting researcher with the Communications Systems and Signal Processing Institute at SDSU, San Diego, CA. Currently, he is a Full Professor and Department Vice Head at the Department of Electronics and Communications Engineering at TUT, Finland. He has been involved in organizing conferences, like the IEEE SPAWC'07 (Publications Chair) held in Helsinki, Finland. His general research interests include communications signal processing, estimation and detection techniques, signal processing algorithms for software defined flexible radios, cognitive radio, digital transmission techniques such as different variants of multicarrier modulation methods and OFDM, radio localization methods, and radio resource management for ad-hoc and mobile networks.